1983SoPh...83...83F

ELECTRIC FIELDS IN CORONAL MAGNETIC LOOPS

P. FOUKAL* and P. MILLER

Atmospheric and Environmental Research, Inc., 872 Massachusetts Avenue, Cambridge, MA 02139, U.S.A.

and

L. GILLIAM

Sacramento Peak Observatory

(Received 10 September, 1981; in final form 22 June, 1982)

Abstract. We analyze spectra taken with the 40 cm coronograph at Sacramento Peak Observatory, for evidence of Stark effect on Balmer lines formed in coronal magnetic structures. Several spectra taken near the apex of a bright post-flare loop prominence show significant broadening from H_{10} to the limit of Balmer line visibility in these spectra, at about H_{20} The most likely interpretation of the increasing width is Stark broadening, although unresolved blends of Balmer emissions with metallic lines could also contribute to the trend. Less significant broadening is seen in 3 other post-flare loops, and the data from 5 other active coronal condensations observed in this study show no broadening tendency at all, over this range of Balmer number. The trend clearly observed in one post-flare loop requires an ion density of $n_i \simeq 2 \times 10^{12}$ cm^{-3}, if it is to be explained entirely as Stark effect caused by pressure broadening. But mean electron densities measured directly from the Thomson scattering at $\lambda 3875$ in the same SPO spectra, yield $\bar{n}_e \lesssim 3\text{–}7 \times 10^{10}$ cm^{-3} for the same condensations observed within that loop. Comparison of this evidence from electron scattering, with densities derived from emission measures and line-intensity ratios, argues against a volume filling factor small enough to reconcile the values of n_i and $\bar{n}_e$ derived in this study. This discrepancy leads us to suggest that the Stark effect observed in these loops, and possibly also in flares, could be caused by macroscopic electric fields, rather than by pressure broadening. The electric field required to explain the Stark broadening in the brightest post-flare loop observed here is approximately 170 V cm^{-1}. We suggest an origin for such an electric field and discuss its implications for coronal plasma dynamics.

1. Introduction

Observations of the high Balmer lines in solar flares have shown that their width increases significantly beyond about H_{10} (e.g. Švestka and Fritzová-Švestková, 1967; Hirayama, 1961). This broadening trend seen in flares, and also to a lesser extent in quiescent prominences (Hirayama, 1963; Jefferies and Orrall, 1958) and in the limb chromosphere (Redman and Suemoto, 1954; Rosenberg *et al.*, 1977; Feldman and Doschek, 1977) has generally been ascribed to pressure broadening in solar plasmas of relatively high ($n_e \gtrsim 10^{12}$ cm^{-3}) density. In all these studies, it was assumed that Stark broadening by *macroscopic* electric fields was negligible, so that the observed dependence of line width upon Balmer number could be interpreted as a direct diagnostic of plasma density.

In this paper we present new evidence on the broadening of the higher Balmer lines, which suggests that strong macroscopic electric fields might be present in coronal

* Visiting Astronomer, Sacramento Peak Observatory.

Solar Physics **83** (1983) 83–102. 0038–0938/83/0831–0083$03.00.
Copyright © 1983 by D. Reidel Publishing Co., Dordrecht, Holland, and Boston, U.S.A.

© Kluwer Academic Publishers • Provided by the NASA Astrophysics Data System

1983SoPh...83...83F

magnetic structures. In Section 2, we describe our observations of the high Balmer lines in a number of active region magnetic loops and coronal condensations, and our reduction of these spectra. In Section 3, we analyze the line widths, and show that the trend with principal quantum number observed in certain of the loops implies a significant Stark broadening contribution. But we also show in Section 4, that the densities required to produce such a large Stark effect by pressure broadening, greatly exceed the densities we determine in the same structures from photometry of the electron scattering continuum, We argue that a volume filling factor small enough to explain this discrepancy appears unlikely from the evidence of other kinds of density measurements in such loops, based on emission measures and line intensity ratios. In Section 5, we compare our results with other electric field measurements in space plasmas. We point out that large scale electric fields of the magnitude implied by the results reported here, could call into question the mhd approximation used to model mass and energy flow in the solar corona.

2. Observations and Reduction

2.1. Description of observational data

The spectra and slit jaw images of coronal magnetic structures analyzed in this study were obtained with the Universal spectrograph and 40 cm coronagraph at Sacramento Peak Observatory. Data subsequently used in this study were obtained during a number of coronal patrol programs between 1969 and 1979. The 1980 and 1981 observations were obtained with pointing and exposures optimized specifically for this investigation.

The spectra have a dispersion of 1.6 Å mm^{-1} in 3rd order at 3950 Å. A spectral region including the wavelength interval between approximately 3600 Å and 4000 Å of interest here, was recorded on exposures of between 10 and 30 s, using 103 AG or 103 D film. Photometrically calibrated slit jaw pictures in Hα were also obtained at a scale of 50μ/arc sec.

Several hundred coronal spectra were examined and 13 were selected for microdensitometry on the basis of Balmer line visibility to at least H_{15}, relatively narrow spectral lines, and acceptable sky background. Table I gives the dates and times of the spectra, along with the McMath number of the active region observed, and a statement on the morphology of the coronal magnetic structure. Our observations include 4 post-flare loop prominences, and also 5 other bright coronal condensations of less well-defined magnetic structure, located over active regions. Two of the latter may be surges, as noted in Table I. For the post-flare loops, we give an estimate of the angle γ between the axis of the loop and the line of sight. Finally, Table I also gives the approximate location of the slit within the coronal structure, measured as a fraction of its projected height d, above the limb.

Figure 1a, b shows Hα slit jaw images of three loops observed in this study. It can be seen that the spatial scale and image quality of these images are adequate for accurate location of the slit relative to the loop structure. Figure 2a shows a sample spectrum,

© Kluwer Academic Publishers • Provided by the NASA Astrophysics Data System

1983SoPh...83...83F

TABLE I

Summary of spectral data

Spectrum	Date	GMT	Active region[a]	Magnetic structure, loop orientation γ and slit location (see Section 2.1)
A	12 Dec. 69	19:48	(M)10477 D	low loop (surge?), $\gamma \sim \frac{\pi}{2}, \frac{z}{d} \sim 0.9$
B	14 Jan. 70	16:21	(M)10514	post-flare loop, $\gamma \sim 0, \frac{z}{d} \sim 1.0$
C	26 Feb. 70	19:19	(M)10614	post-flare loop, $\gamma \sim \frac{\pi}{8}, \frac{z}{d} \sim 1.0$
D	11 Aug. 72	13:47	(M)11976	post-flare loop, $\gamma \sim \frac{\pi}{2}, \frac{z}{d} \sim 0.5$
E[b]	11 Aug. 72	13:47	(M)11976	post-flare loop, $\gamma \sim \frac{\pi}{2}, \frac{z}{d} \sim 0.5$
F	11 Aug. 72	13:59	(M)11976	post-flare loop, $\gamma \sim \frac{\pi}{2}, \frac{z}{d} \sim 0.5$
G	11 Aug. 72	14:19	(M)11976	post-flare loop, $\gamma \sim \frac{\pi}{2}, \frac{z}{d} \sim 0.8$
H	11 Aug. 72	14:47	(M)11976	low loop (surge?) $\gamma \sim \frac{\pi}{2}, \frac{z}{d} \sim 0.9$
I	11 Aug. 72	14:48	(M)11976	low loop (surge?) $\gamma \sim \frac{\pi}{2}, \frac{z}{d} \sim 0.9$
J	1 May 73	13:48	(M)12322	post-flare loop, $\gamma \sim \frac{\pi}{4}, \frac{z}{d} \sim 1.0$
K	5 Nov. 79	16:07	(M)16415	active condensation
L	1 Feb. 81	21:44	(B)2903	active condensation
M	2 Feb. 81	16:17	(B)2927	active condensation

[a] M, B, represent the McMath and Boulder active region numbers, respectively.
[b] Spectra D, E represent two spatially separate regions scanned with the microdensitometer in this loop spectrum.

taken of the brightest region located near the apex of the post-flare loop shown in Figure 1a. The Balmer lines are clearly visible to H_{20} and beyond. In this very bright loop, observed under exceptionally good conditions of sky background, electron scattering continuum is easily seen.

© Kluwer Academic Publishers • Provided by the NASA Astrophysics Data System

1983SoPh...83...83F

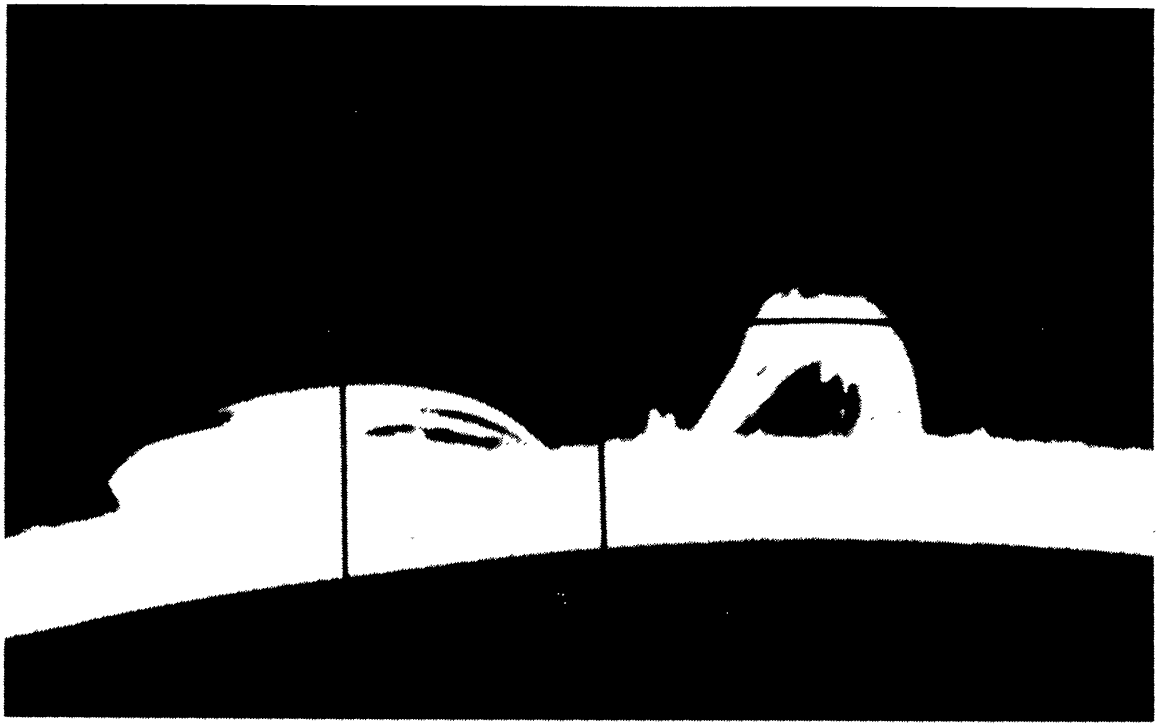

a)

b)

Fig. 1. Hα slit jaw images of (a) the post-flare loop and low surge loop of 11 August, 1972, at GMT 14 : 19. The curved spectrograph slit is oriented parallel to the limb, and intersects the post-flare loop near its apex, in this pointing. The spectrograph slit does not intersect the low loop (spectra H, I) in this pointing. Two parallel dark fiducial lines intersect the limb and slit at approximately a right angle. Their spacing corresponds to 55 000 km. The second image (b) shows the post-flare loop of 1 May, 1973. The slit intersects the two brightest condensations near the apex.

© Kluwer Academic Publishers • Provided by the NASA Astrophysics Data System

1983SoPh...83...83F

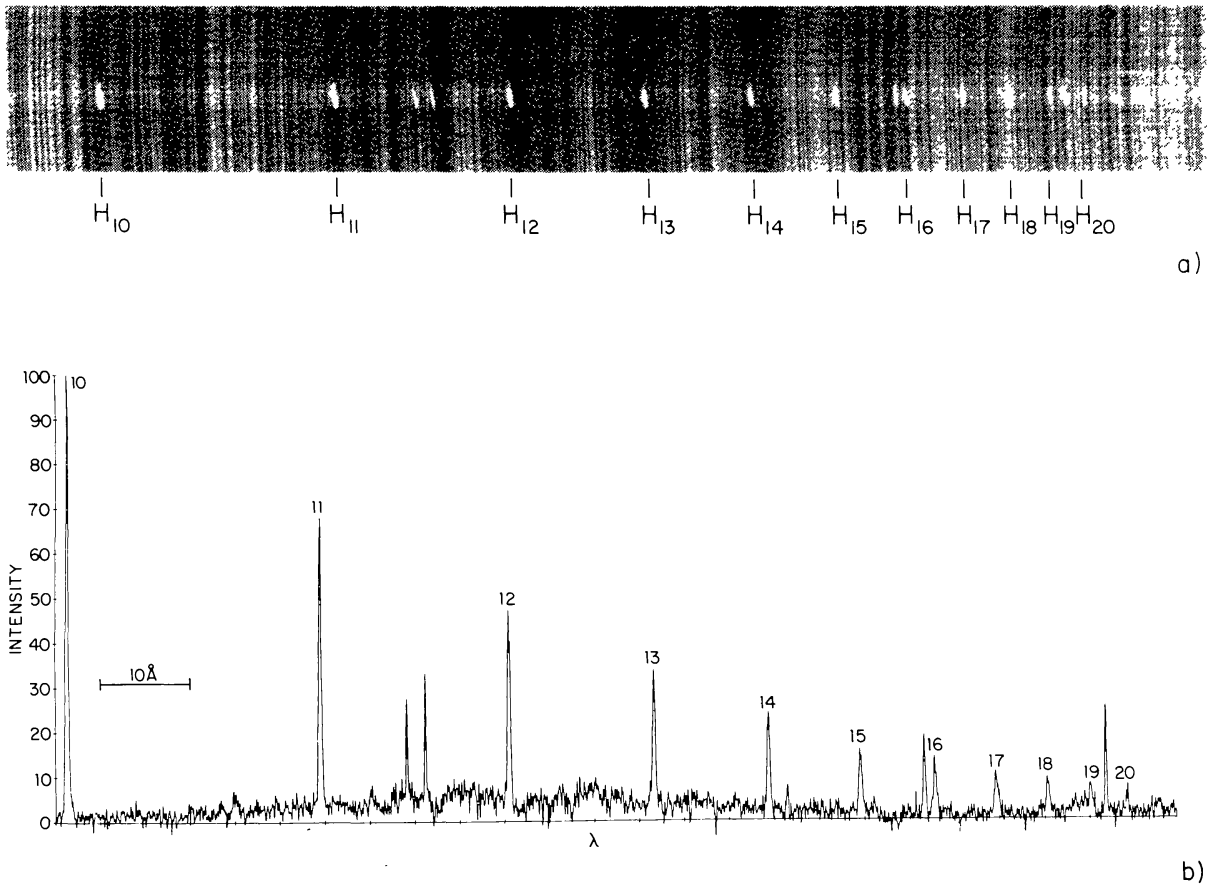

Fig. 2. A sample spectrum showing the wavelength region between 3800 and 3600 Å. This spectrum was taken on 11 August, 1972 at GMT 14 : 19 at the same pointing near the apex of the post-flare loop illustrated in Figure 1a. In (a) we show a spectrogram illustrating the Balmer lines H_{10} to beyond H_{20}. The Thomson continuum is also clearly visible. In (b) we show a linear intensity scan across the center of this spectrum, between H_{10} and H_{20}, with the background subtracted.

2.2. Determination of the Balmer Line Halfwidths

The spectra described in Table I were scanned with a microdensitometer from H_7 (λ3970.1) to beyond H_{20} (λ3628.8). Figure 2b shows a portion of such a scan across the spectrum shown in Figure 2a, over the wavelength interval between H_{10} and H_{20}. Each spectrum was also scanned a second time, along a line displaced from the bright condensations seen in the Balmer emissions. This background was subsequently subtracted from the spectral scan to remove the Fraunhofer absorption line spectrum scattered from the sky, which is the main source of noise. The subtracted scans were smoothed with a Gaussian filter of 0.065 Å halfwidth to reduce high frequency emulsion noise.

The total instrumental profile was taken to be a Gaussian, with a full width at half intensity calculated as 0.103 Å. This width was found from convolution of the smoothing filter profile given above, with the slit and microdensitometer aperture profiles of 0.073 Å and 0.033 Å halfwidths, respectively.

© Kluwer Academic Publishers • Provided by the NASA Astrophysics Data System

1983SoPh...83...83F

2.3. Determination of the Thomson continuum intensities

Microdensitometer scans were also made transverse to the dispersion direction in a spectral region free of lines near $\lambda 3875$, to measure the intensity of the electron scattering continuum. In all the coronal structures observed excepting the two post-flare loops illustrated in Figure 1, the intensity of this continuum was found to be below the level of grain noise and inhomogeneities in background caused by scattering from slit imperfections.

Determination of intensity in this continuum (or an upper limit based on noise in the background) requires absolute calibration of the transmission wedge values. This is achieved by illuminating the wedges through a diffusing screen whose surface brightness is known to be a factor 2.6×10^{-4} at $\lambda 3875$, below the mean intensity of the solar disc.

3. Analysis of the Balmer Line Widths

3.1. The measured Balmer line widths

The full widths at half intensity $\Delta\lambda_{1/2}$, of the Balmer lines H_7 through H_{20} were measured from tracings such as Figure 2b, for the 13 spectra studied. These halfwidths are plotted against upper principal quantum number n, in Figure 3. Figure 3a shows the behavior of the halfwidths measured from the 4 spectra (D–G, Table I) obtained of the post-flare loop observed on 11 August, 1972, that is illustrated in Figure 1a. The curve in Figure 3a represents a quadratic least squares fit to these data, taken to be of equal weight. We note that the minimum values of $\Delta\lambda_{1/2} \simeq 0.3$ Å are approximately three times larger than

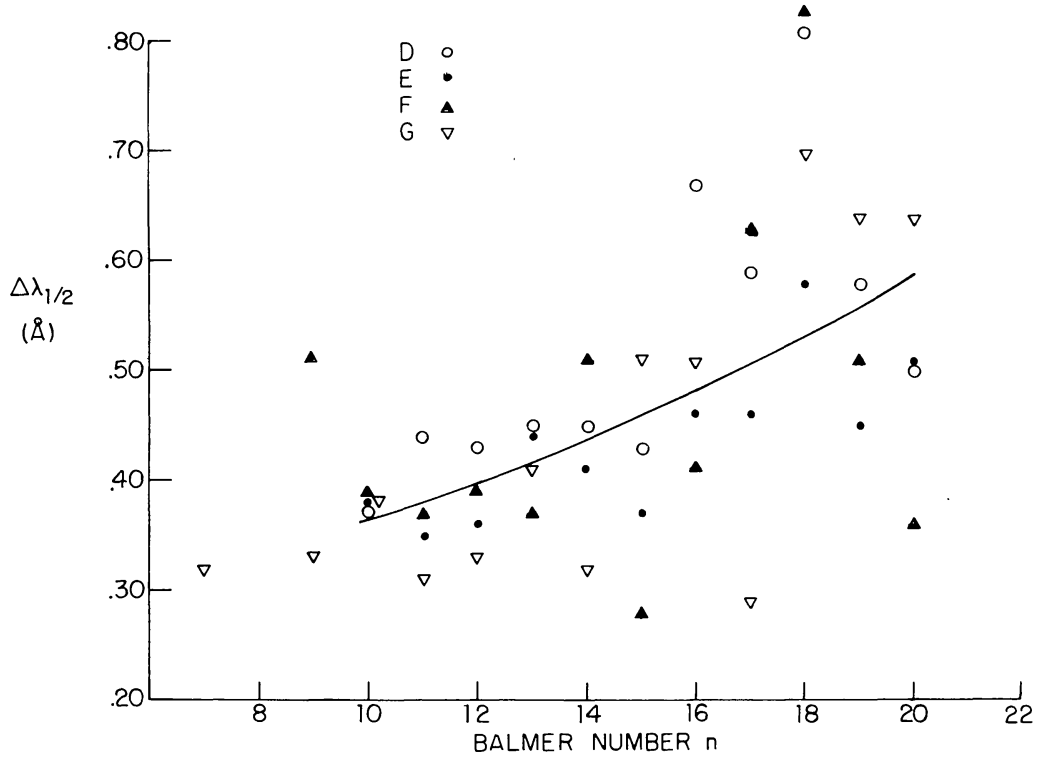

Fig. 3a.

© Kluwer Academic Publishers • Provided by the NASA Astrophysics Data System

1983SoPh...83...83F

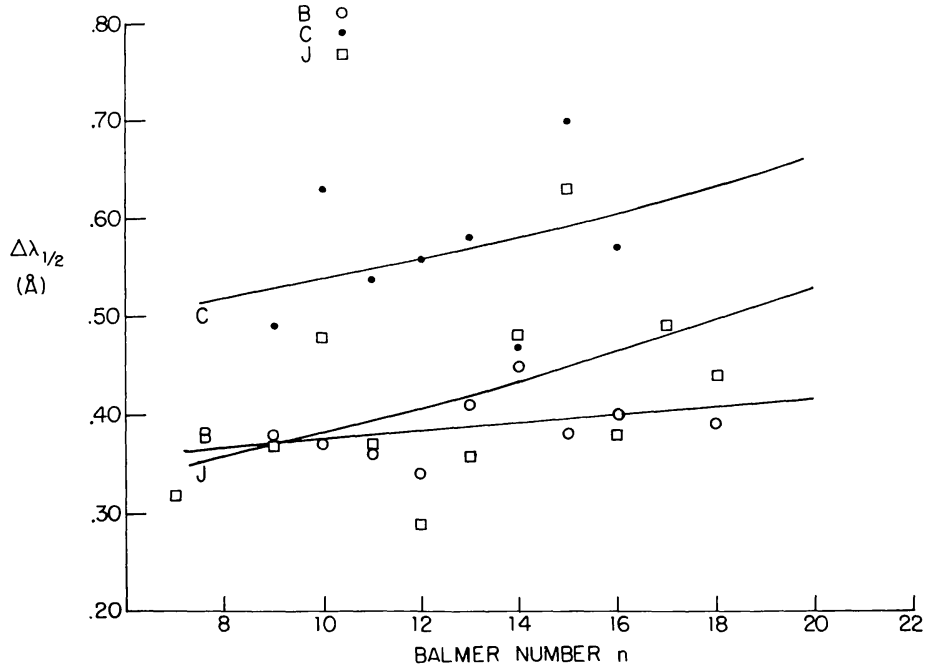

Fig. 3b.

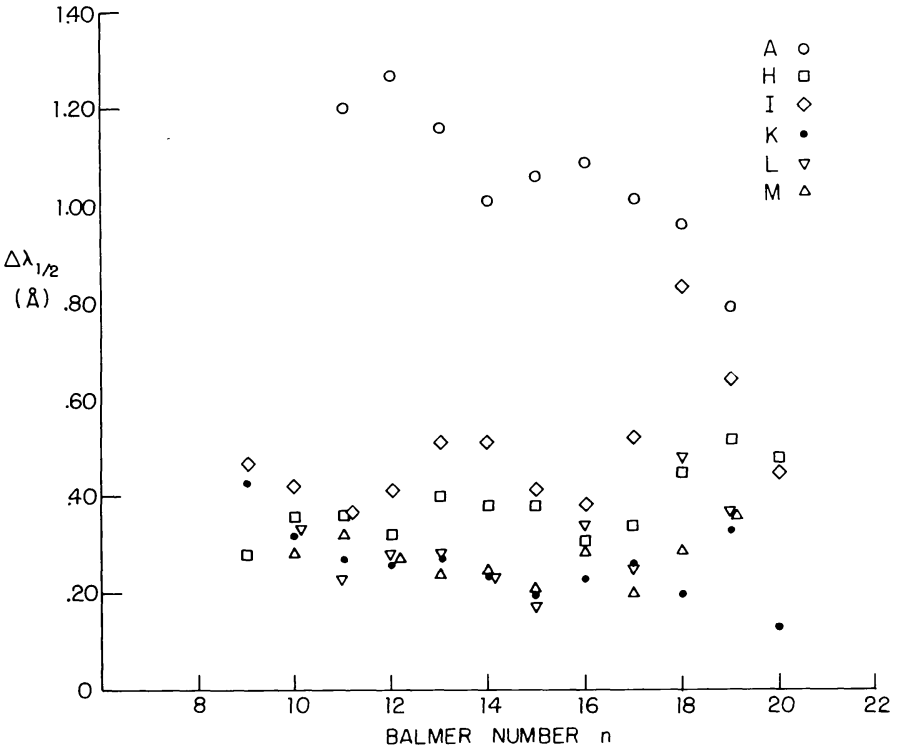

Fig. 3c.

Fig. 3a–c. Plot of $\Delta\lambda_{1/2}$ against Balmer number n, for (a) the four spectra recorded on the 11 August, 1972 post-flare loop. Plot (b) represents measurements of $\Delta\lambda_{1/2}$ from three spectra of three other individual post-flare loops. The curves represent least squares fits to the data for each individual loop, in both plots. Plot (c) gives the behavior of $\Delta\lambda_{1/2}$ for 5 other coronal loops and condensations.

© Kluwer Academic Publishers • Provided by the NASA Astrophysics Data System

1983SoPh...83...83F

the instrumental halfwidth. A second point is that the observed dispersion of $\Delta\lambda_{1/2}$ for given n significantly exceeds experimental errors, particularly at low n, since the low Balmer lines in this loop are bright and easily measured (see Figure 2). This shows that small differences in pointing within the loop and also in alignment of the microdensitometer scans, can yield significant variations in $\Delta\lambda_{1/2}$. Despite the random variation, the halfwidths in this loop show a clear broadening trend with increasing n. From the least squares curve, the difference in width between H_{10} and H_{20} is approximately 0.2 Å. The interpretation of this broadening is considered in detail below.

Figure 3b gives the halfwidths measured from the 3 spectra (B, C, and J) of 3 other post-flare loops. One of these loops, observed on 1 May, 1973, is illustrated in Figure 1b. The Balmer lines in these loops were only measurable to between H_{16} and H_{18}. We note that the halfwidths at $n < 15$ in spectrum (C) are considerably larger than in either of the spectra (B) or (J), or in the data given in Figure 3a. There is no obvious explanation in terms of macroscopic mass motions for these much broader Balmer lines, since we find no connection between either this loop's orientation, or of the slit location within it, as compared to the narrower spectra. Quadratic least squares fits to the halfwidth data for these three loops individually show weak evidence for small increases in width between H_{10} and the highest measurable Balmer line at H_{18} or H_{16}.

Figure 3c shows the halfwidths from 3 spectra of two low loops, possibly surges (spectra A, H, I) and from 3 spectra (K, L, M) of 3 other active coronal condensations. One of the low loops is illustrated in Figure 1a. None of these spectra show any tendency for Balmer line broadening with n. In one of the low loop spectra (A), the lines are extremely broad and show a tendency to decrease in width at higher n.

In Sections 3.2 to 3.5 we discuss the most likely physical explanations of the variable excess Balmer line broadening in these coronal magnetic structures. In Section 3.6 we discuss the broadening trend with increasing n, that is observed in some cases.

3.2. Fine structure of the Balmer lines

The fine structure splitting of the nth hydrogen energy level is proportional to $1/n^3$. It follows that the splitting of the higher levels of $n \geq 7$ is negligible relative to that of the Balmer ground level $n = 2$. Thus we expect an effectively constant wavelength splitting of the high Balmer doublets, caused only by the energy separation between the ^2S and

1983SoPh...83...83F

where k is the Boltzmann constant. In our calculations, we take $T = 6000$ as the formation temperature of the Hα line core (e.g., Vernazza *et al.*, 1981). The Balmer line halfwidth due to thermal motions alone at this temperature, is found from Equation (1) to be 0.21 Å.

A numerical convolution of the profiles produced by fine structure together with thermal and instrumental broadening, yields a total halfwidth $\Delta\lambda_{1/2}$ of 0.34 Å. These three factors suffice to explain the mean width of the narrowest Balmer lines measured in these loops. For this reason we set $v = 0$ in the calculation of our line profiles. The effect of setting $v = 0$ upon the density derived from Stark effect is discussed in Section 3.6. Clearly microturbulence may play a role in explaining the very broad lines of spectra A and C.

Besides the three factors above which must act, and appear sufficient to explain the narrowest lines, we mention three additional influences that may contribute to produce halfwidths in excess of 0.50 Å observed in some of the loops.

3.4. Optical depth of the high Balmer lines

Previous studies of the Balmer widths in prominences (Hirayama, 1963; Jefferies and Orrall, 1958) and flares (Švestka and Fritzová-Švestková, 1967) indicate that the width is least around H_{10}. The increase of width with decreasing n below H_{10} is attributed to increasing optical depth. Since we find good correspondence between the mean observed and calculated halfwidths around H_{10}, it is reasonable to assume that self-absorption is negligible beyond H_{10} in these loops. However, we might expect that the opacity of somewhat larger, denser or cooler loops might exceed the mean conditions. We estimate that a hydrogen density of at least 10^{11} cm^{-3} would be required to yield unity optical depth at H_{20} in loop structures of $D \sim 10^4$ km (taking the relative level population $n_2/n_1 \sim 10^{-6}$ at $T = 7 \times 10^3$ K and $n_H \sim 10^{11}$ from Vernazza *et al.* (1981)). This could contribute to the larger line widths observed in certain spectra. Decreasing optical depth is the most reasonable explanation of the decreasing widths seen in the spectrum (A).

3.5. Blending of the Balmer lines

Table II gives the (laboratory) wavelengths of the Balmer lines H_8 to H_{20}. This table also lists possible blends with lines of heavier elements, based on the extensive analysis of chromospheric eclipse spectra obtained at a dispersion of about 2 Å mm^{-1} by Dunn *et al.* (1968). For instance, the blend of H_8 with the (often stronger) He I 3888.65 line, is partially resolved in our spectra. We have not attempted to measure the H_8 halfwidth at all in this analysis on account of this blending.

Judging from the list of Dunn *et al.* (based on possible blends unresolved in their spectra), only H_9, H_{10}, and H_{16} of the lines studied here are not blended. Examination of the most homogeneous set of data on one loop in Figure 3a, shows no evidence that those three lines behave differently as a group than the others. On the other hand, we do suspect that blending contributes to the unusual width of H_{18}.

© Kluwer Academic Publishers • Provided by the NASA Astrophysics Data System

1983SoPh...83...83F

TABLE II

Balmer lines measured in this study and some possible blends listed by Dunn *et al.* (1968)

Balmer line	Laboratory wavelength Å	Suggested blends
H_8	3889.05	He I 3888.65
H_9	3835.39	none (± 1.0 Å)
H_{10}	3797.90	none (± 1.0 Å)
H_{11}	3770.63	Ti I 3771.65
H_{12}	3750.15	Fe I 3749.49
H_{13}	3734.37	Fe I 3734.87
H_{14}	3721.94	Ti II 3721.63
H_{15}	3711.97	Cr II 3712.97
		Fe I 3711.23
H_{16}	3703.86	none (± 1.0 Å)
H_{17}	3697.15	Zr II 3698.17
H_{18}	3691.56	Er II 3692.64
		Fe I 3690.73
H_{19}	3686.83	Fe I 3686.00
		Fe I 3687.46
H_{20}	3682.81	Fe I 3682.23

We believe that blending alone is unlikely to account for the systematic broadening trend seen in Figure 3a. But changing blends in loops of different excitation conditions might account for some of the real dispersion in widths observed in this study. Unfortunately, it is difficult to predict a priori whether a blend should increase or decrease the measured $\Delta\lambda_{1/2}$ of a particular Balmer line.

3.6. Stark effect due to pressure broadening and macroscopic electric fields

As pointed out in a number of previous studies (Ivanov-Kholodnyi, 1969; Švestka and Fritzová-Švestková, 1967) the increasing width of Balmer lines with n in certain flare and chromospheric spectra is most reasonably explained by the Stark effect. Of the broadening mechanisms described above, only Stark effect can account for a systematic increase of halfwidth with n.

Pressure broadening under astrophysical conditions has been discussed by Griem (1960, 1974). Following the treatment of Griem (1974) we base our calculations of the Stark profile $S_{nn'}(\alpha)$ (for a transition between upper state n and lower state n') on the Holtsmark (1919) theory of broadening by protons in the quasi-static approximation. Here we use as variable the normalized line-center distance $\alpha = \Delta\lambda/E_0$, defined in terms of the Holtsmark field strength

$$E_0 = 2.61 e n_i^{2/3}, \tag{2}$$

with e the electron charge in esu. The additional broadening by electrons is treated as a correction to the above profile, derived on the impact approximation for electrons. This correction as used in our analysis is described in Appendix A.

© Kluwer Academic Publishers • Provided by the NASA Astrophysics Data System

1983SoPh...83...83F

Our calculation departs from that of Griem (1974, p. 237) in the respect that our representation of the line core is taken from the profiles of Balmer lines tabulated individually to H_{18} by Underhill and Waddell (1959). These profiles tabulated as a function of the variable α, take explicit account of the Stark effect on individual fine structure components of the line, using the Holtsmark theory. We have found that this procedure is noticeably more accurate than use of an arbitrary function to represent the line core, as suggested by Griem.

The computed functions $S_{nn'}(\alpha)$ were convolved numerically with the line profile resulting from instrumental and thermal broadening described above. The computed total halfwidths $\Delta\lambda_{1/2}$ are plotted against n in Figure 4, for the three cases of ion densities $n_i = 5 \times 10^{11}$, 1×10^{12}, and 3×10^{12} cm^{-3}. In computing these profiles, we have set the microturbulence velocity $v = 0$. This approach is conservative in the sense that it tends to underestimate the density required to match the slopes of the observed curves in Figure 4.

Figure 4 also includes two least squares fits to the observations of the 4 post-flare loops. One curve representing observations of the 11 August, 1972 loop is taken directly from Figure 3a. A second curve represents the mean broadening trend found in the other 3 post-flare loops, for which individual data are given in Figure 3b. To obtain a curve describing the dependence of $\Delta\lambda_t$ on n in these three loops, we have adjusted the values

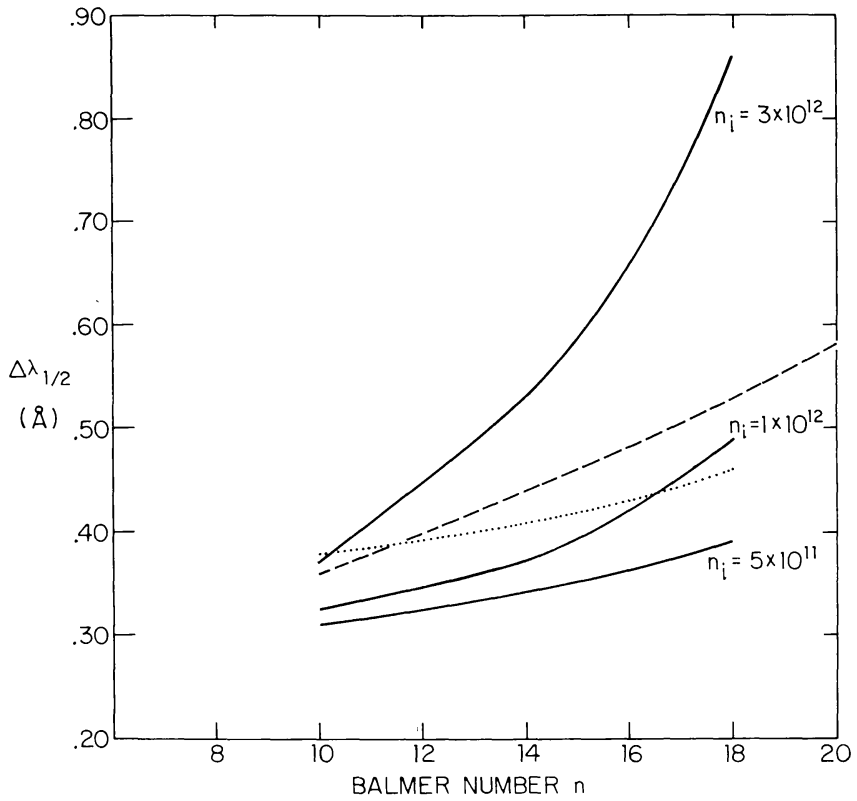

Fig. 4. Calculated values of the total halfwidth $\Delta\lambda_{1/2}$ plotted (solid line) against Balmer number n, for ion plasma densities of $n_i = 5 \times 10^{11}$, 1×10^{12}, and 3×10^{12} cm^{-3}. The dashed line represents the curve of observed values of $\Delta\lambda_{1/2}$ for the 11 August, 1972 loop, taken from Figure 3a. The dotted line represents observed values for 3 loops taken from Figure 3b, as explained in the text.

© Kluwer Academic Publishers • Provided by the NASA Astrophysics Data System

1983SoPh...83...83F

of $\Delta\lambda_t$ for the spectrum (C) downward, to bring their center of gravity into coincidence with that for the other two loops, whose average line width is much narrower. The second curve plotted in Figure 4 then represents the least squares fit to these adjusted, equally weighted data.

We see from Figure 4 that if pressure broadening alone is responsible, a density of approximately 2×10^{12} cm^{-3} is required to match the slope of the 11 August, 1972 data. A lower density of between 5×10^{11} and 1×10^{12} cm^{-3} would be consistent with the less significant slope found in the combined data from the 3 other post-flare loops.

A closer match to the observed widths at H_{10} can be achieved by adopting a turbulent velocity $v = 7.5$ km s^{-1}. But we do not believe that such tuning of the calculated curves is significant, in view of the obvious uncertainties in this procedure, and also our neglect of small broadening terms such as the anomalous Zeeman effect for the Balmer lines.

Alternatively, the slopes in the data of Figure 4 could arise from the Stark effect of a macroscopic electric field. From the quasi-static approximation (ignoring electron contributions and particle correlations) we have for the intensity E of this field (Griem, 1974, p. 22)

$$E \approx 8.8\, e\, n_i^{2/3}\,, \tag{3}$$

where e is the electron charge in esu, and n_i is the particle density (cm^{-3}) of singly charged ions. The electric field corresponding to the density $n_i = 2 \times 10^{12}$ cm^{-3}, derived from Equation (3) is 167 V cm^{-1}.

4. The Plasma Density in Post-Flare Loops

4.1. Evidence from Thomson scattering in the SPO spectra

The intensity I_s of the (optically thin) electron scattering continuum measured here at $\lambda 3875$ can be related to the mean electron density $\bar{n}_e$ over the path length L through the loop, by the formula:

$$I_s = \frac{6.6 \times 10^{-25}}{4\pi}\, \bar{n}_e L \int^{\omega} 3/4(1 + \cos^2\psi) I(\omega)\, \mathrm{d}\omega\,. \tag{4}$$

Here $I(\omega)$ is the photospheric intensity at $\lambda 3875$ incident upon the loop, ω is the solid angle subtended by the photosphere at the scattering electron, and ψ is the angle at the electron between the incident and scattered beam.

A good approximation to Equation (4) can be derived that is adequate for our purposes (Appendix B). For a loop height $h = 5 \times 10^4$ km, this yields an upper limit to $\bar{n}_e$ given by

$$\bar{n}_e \lesssim \frac{1.3 \times 10^{25}}{L}\, I_s/\bar{I}_\odot\,, \tag{5}$$

© Kluwer Academic Publishers • Provided by the NASA Astrophysics Data System

1983SoPh...83...83F

TABLE III

Measurements on the electron scattering continuum and Hα slit jaw images

Spectrum	$I_s/\bar{I}_\odot (\times 10^{-6})$	D(km $\times 10^4$)	$\bar{n}_e$(cm^{-3} $\times 10^{10}$)
A	< 3.9	0.7	7
B	–	0.6	–
C	< 10	0.6	< 22
D	6.0	1.2	7
E	2.5	1.1	3
F	5.6	1.3	6
G	2.8	1.3	3
H	3.0	0.6	7
I	2.0	0.6	5
J	3.6	0.7	7
K	–	1.4	–
L	–	1.4	–
M	< 15	2.8	< 7

where I_s and $\bar{I}_\odot$ are respectively the scattered intensity and mean intensity of the solar disc. Since our interest lies in determining whether the plasma density in loops can be as large as values required to produce the observed Stark effect, the upper limit defined by Equation (5) is sufficient for this analysis.

Table III gives the intensity ratios $I_s/\bar{I}_\odot$, derived from our photometry, for 10 of the spectra studied. Table III also gives values of D, the projected diameter of the loops, measured with a micrometer from the Hα slit jaw images. Upper limits to $\bar{n}_e$ are then derived from Equation (5), assuming that the loop is cylindrical and the path length along a chord L through the structure can be approximated as $L \sim D$.

We see from Table III that the densities for the two loops (11 August, 1972 and 1 May, 1973) where electron scattering continuum can be measured, are in the range $\bar{n}_e \lesssim 3\text{–}7 \times 10^{10}$ cm^{-3}. This result is similar to that found by Fisher (1975) in an independent determination of the electron scattering density in the 11 August, 1972 loop. In the remaining 3 objects where good calibrations were available, only upper limits to $I_s/\bar{I}_\odot$ can be derived. These place upper limits to the mean density in the broad range $\bar{n}_e < 2\text{–}22 \times 10^{10}$ cm^{-3}.

4.2. Densities from Emission Measures and Line Intensity Ratios

A root-mean square estimate of the density in the Balmer-line emitting plasma can be obtained from the intensities of the highest observable Balmer lines, extrapolated to the series limit. The intensity $I_{2,\infty}$ at the series limit can be related to the emission measure through the formula (see e.g., Jefferies and Orrall, 1961)

$$I_{2,\infty}\, d\lambda = 4.8 \times 10^{-15}\, d\lambda \int n_p n_e T_e^{-3/2}\, dz\,. \tag{6}$$

Absolute calibration of the spectra $(D - I)$ for the 11 August, 1972 loop yields an intensity of the highest measurable Balmer line (H_{22}) of $I_{22} \sim 60$ erg sr^{-1} cm^{-2} s^{-1} (0.25 Å)$^{-1}$. Assuming $T_e = 1 \times 10^4$ K and $n_p = n_e$ = constant over the path length

© Kluwer Academic Publishers • Provided by the NASA Astrophysics Data System

1983SoPh...83...83F

$\int dz = D \sim 1 \times 10^9$ cm of that loop (see Table III), and with $d\lambda = 1$ cm, we then find an upper limit of $\langle n_e \rangle < 7 \times 10^{10}$ cm^{-3}, since $I_{22} > I_{2,\infty}$.

No emission measures from EUV resonance lines or X-rays are available for any of the loops studied here. However, such measurements are available for post-flare loops observed during the Skylab emission. Thus, Petrasso *et al.* (1979) find $\langle n_e \rangle$ in the range (5.4 to 7.3 ± 2) $\times 10^9$ in the brightest condensations seen in soft X-rays near the apex of a bright post-flare loop on July 29, 1973. Foukal (1978) and Cheng (1980) have reported similar densities, in the range 4×10^9 to 1×10^{10} in coronal lines, in the brightest condensations of several post-flare loops observed in the EUV. Somewhat lower densities are found in EUV transition region lines formed at temperatures as low as 3×10^4 K (C II λ1335) in the same loops.

The EUV and X-ray emission measures taken as a whole indicate densities about a factor five lower than the upper limit derived above from the Balmer line intensities. Some of this difference may be attributed to the unusual brightness of the 11 August, 1972 post-flare loop. But it may also indicate higher values of n_e in the coolest plasma. Equation (6) is derived on the assumption that the population of the highest hydrogen levels near the series limit is in LTE with the population of ionized hydrogen. Calculations of hydrogen level populations in quiescent prominences of similar temperature and density indicate this assumption is probably valid to better than a factor two (A. Poland, private communication), in the loops studied here.

In the derivations of $\bar{n}_e$ and $\langle n_e \rangle$ above, we have assumed that the volume filling factor of the plasma occupying the loop is unity. In fact, this is unlikely to be the case, and the relative magnitudes derived for $\bar{n}_e$ and $\langle n_e \rangle$ using this assumption actually carry information on the true filling factor and thus, on the true local density in the plasma condensations. In the simplest physically reasonable model, we may suppose that the electrons producing Thomson scattering occupy a fraction $\varepsilon \leq 1$ of the total path length D, while the plasma responsible for a line radiation used to derive a value of $\langle n_e \rangle$ occupies the fraction ε'. Since all the plasma contributes to the scattering, but only a certain temperature regime can contribute to each of the measured line emissions, we require $\varepsilon' < \varepsilon$. We also assume in this model that all the plasma in the condensations has the same true density n_e. It can then easily be shown (e.g., Foukal, 1978) that

$$\bar{n}_e / n_e = \varepsilon \tag{7}$$

and

$$\langle n_e \rangle / n_e = (\varepsilon')^{1/2} . \tag{8}$$

Equations (7), (8) imply that $\varepsilon' \leq \varepsilon^2$ (or $\varepsilon' \leq \varepsilon$ since $\varepsilon \leq 1$), as required above, provided $\bar{n}_e \geq \langle n_e \rangle$. This is consistent with our observations, since $\bar{n}_e$ was found above (Table III) to be in the range $3\text{–}7 \times 10^{10}$ cm^{-3}, while $\langle n_e \rangle$ ranged between $0.5\text{–}7 \times 10^{10}$ cm^{-3}.

Our model introduces three unknowns into the two Equations (7) and (8), so that we cannot expect to derive a firm estimate of n_e from our observations of $\bar{n}_e$ and n_e alone. But we draw attention to the fact that a filling factor $\varepsilon' = 1.2 \times 10^{-3}$ is required to reconcile the Balmer line emission measure density $\langle n_e \rangle$ with a Stark broadening

© Kluwer Academic Publishers • Provided by the NASA Astrophysics Data System

1983SoPh...83...83F

density of $n_e = 2 \times 10^{12}$ cm^{-3}. This filling factor would imply that all the Balmer emission along the line of sight arises from a path length of only 10 km.

A direct measurement of the local electron density n_e can be obtained from the intensity ratios of certain density-sensitive lines. A measurement using the Ca XV forbidden line ratio $I(5694)/I(5445)$ has been reported by Fisher (1975) in the same 11 August, 1972 loop studied in this paper. His value of $n_e \sim 1 \times 10^{11}$ is close to that derived from electron scattering by him and in this paper. We note that this line ratio does not appear to saturate until densities in excess of 10^{12} are reached (Chevalier and Lambert, 1970). The Ca XV lines are formed at $T_e \sim 5 \times 10^6$ K, so it is not clear that they measure a local density n_e that can easily be related to that found in the cooler Balmer-line emitting regions. But it seems that if the true local density in the hot plasma were really a factor 20 lower than that in the Balmer emitting volumes, we would expect by Equation (8) a factor 20 higher value of $\langle n_e \rangle$ at these lower temperatures, unless the filling factor decreased by 1/400. Observations of the emission measures in radiations formed between $T \sim 2 \times 10^6$ K and $T \sim 3 \times 10^4$ K (Foukal, 1978; Cheng, 1980; Dere, 1982), (including the Balmer lines analyzed above), show quite consistent emission measure densities from these post-flare loops. This suggests that the value of $n_e \sim 1 \times 10^{11}$ cm^{-3} obtained from the Ca XV ratio does argue against a density as high as 2×10^{12} cm^{-3} in the cool plasma.

5. Discussion and Conclusions

We find in this study that the Stark effect identified in at least one of the post-flare loops analyzed, seems too large to be explained in terms of pressure broadening. We are led to this conclusion by analysis of the density in that same loop by three independent diagnostics besides the Stark effect. None of these three diagnostics (electron scattering, emission measures and the Ca XV line intensity ratio) measure the true local density in the Balmer line emitting plasma. But we find that a rather small volume filling factor, and also a very rapid increase in that filling factor with plasma temperature, are required to reconcile the much lower values of $\bar{n}_e$, $\langle n_e \rangle$, and n_e (Ca XV) with a value of $n_e \sim 2 \times 10^{12}$ cm^{-3} required to explain the Stark effect by pressure broadening alone.

This evidence leads us to conclude that a macroscopic electric field of intensity reaching $E_0 \sim 170$ V cm^{-1} is likely to be present in the condensations near the top of post-flare loops. Some evidence for the existence of large scale electric fields in the solar corona has been previously put forward by Davis (1977), based on intensity ratios of allowed and forbidden He I triplet lines in flares, and by Jordan *et al.* (1980), based on line shifts of high order Si I lines in sunspots. The electric fields estimated in those studies are several times larger than the values derived here.

A macroscopic electric field of the magnitude inferred in our study raises some basic questions about the plasma dynamics of coronal magnetic loops. For one, our observations show Stark broadening over a large and spatially resolvable region located near the top of post-flare loops. The spatial extent and emission measure of this region appear to be far too large to be identified with a thin sheath of anomalously low electrical

© Kluwer Academic Publishers • Provided by the NASA Astrophysics Data System

1983SoPh...83...83F

conductivity and relatively large electric field predicted from models of magnetic reconnection after flares (e.g., Kopp and Pneuman, 1976). We are forced to consider processes that might lead to large scale d.c. or wave-related electric fields occupying a large fraction of the loop volume.

In principle, a large-scale electric field might be associated with plasma translation across magnetic field lines at a rate of transverse flow given by

$$v_\perp = \frac{cE}{B} , \tag{9}$$

where c is the light speed in cm s^{-1} and B is the magnetic field intensity in gauss. Taking $E \sim 0.1$ esu and $B = 5 \times 10^2$ g, we find $v_\perp \sim 6 \times 10^6$ cm s^{-1}. It is interesting to note that an inflow of matter into 'closed' magnetic loops at about this rate has previously been inferred from studies of the mass and energy balance of post-flare loops (e.g., Kopp and Pneuman, 1976; Foukal, 1978).

But the dynamics of such a motion is difficult to understand within the scope of the magnetohydrodynamic approximation conventionally used to model mass flow in the solar atmosphere. For instance, we might visualize the observed electric field as the result of an external force driving plasma across the loop field lines. The rather large external force driving this flow against the Lorentz force $\mathbf{j} \times \mathbf{B}$ might conceivably be identified with stresses arising from emergence of an active region loop into previously existing coronal magnetic fields. However, even if a sufficiently large driving force were identified, it is still difficult to understand such a large relative motion $v_\perp$ within the MHD approximation, in view of the enormous self-inductance of the plasma loop. Regardless of the magnitude of the driving force, the size of $v_\perp$ is limited by the magnetic Reynolds number implied by the motion, to values many orders of magnitude below that implied by Equation (9). For these reasons, we do not believe that the electric field inferred here can be understood in terms of a $\mathbf{v} \times \mathbf{B}$ drift field driven by large external forces, through a uniformly highly conducting medium.

However, we point out that the observed electric field and drift velocity might be reasonably explained if the tenuous medium outside the loop itself were a relatively *poor* electrical conductor (for instance an essentially pure vacuum). In this case motions of plasma transverse to the loop field would merely produce a polarization electric field across the magnetic field lines. If the circuit thus established could not draw a steady current through the outside vacuum, no steady $\mathbf{j} \times \mathbf{B}$ force could oppose motion of the plasma across the field. Only a very modest driving force (e.g., gravity) might suffice in this case to produce values of $v_\perp$ and thus $\mathbf{E} = (\mathbf{v} \times \mathbf{B})/c$ of the magnitude discussed above*. We point out in this connection that the recent discovery of large-scale magnetic field-aligned (E_{11}) electric fields in the magnetosphere (see, e.g., review by Stern, 1977)

* The field $E = \mathbf{V} \times \mathbf{B}/C$ is felt by an atom in whose rest frame the velocity $\mathbf{V}$ is measured (not by an atom moving at the velocity $\mathbf{V}$ across the magnetic field). Consequently the Stark effect measured here implies an electric field generated by plasma condensations moving at velocity $\mathbf{V}$, but impressed on a surrounding hydrogen atmosphere of the loop that is not itself comoving with those condensations.

© Kluwer Academic Publishers • Provided by the NASA Astrophysics Data System

1983SoPh...83...83F

has led to re-examination of the postulate of high conductivity in tenuous space plasmas (see also Alfvén, 1977).

A d.c. electric field of 170 V cm^{-1} exceeds the critical runaway electric field calculated for these temperatures and densities, by two orders of magnitude. If this large d.c. electric field were imposed parallel to the loop's magnetic field, turbulence would probably result. The influence of turbulence upon the transport coefficients important for energy balance of the loop plasma, has been considered in detail by Hinata (1979). In the case of interest here, the polarization electric field $E_\perp$ is imposed across the magnetic field lines, so the significance of the critical runaway electric field is less clear. The main point is that the size of d.c. field derived here should not be considered implausible simply on the grounds that it exceeds the critical runaway value.

A physically reasonable current path that is consistent with the magnitude of $E_\perp$, location in the loop and spatial dimensions of the electric field region described here, has been put forward by Hinata (1981). More observations are clearly required before the presence of macroscopic electric fields in coronal loops can be considered as firmly established. Simultaneous and co-spatial observations of the Balmer line Stark effect and also of non-saturating line ratio density diagnostics (such as Ca XV λ5694, λ5445) in several bright loops, is of the most immediate importance to study the possible presence of a very large volume filling factor in the loop plasma. More information on the types of loops that show Stark broadening, and on its behavior as a function of position within the loop, would be desirable. Additional information on the vector behavior of the field might be obtained through careful study of the Balmer line polarization patterns, using a Stokes polarimeter.

Acknowledgements

We thank S. Hinata, J. Jefferies, and Z. Švestka for useful comments on this paper. We are also grateful to W. Waller and B. Greene at AER for their careful assistance in microdensitometry of the spectra. This work was supported at AER under NSF grant AST–7923232. Sacramento Peak Observatory is operated by the Association of Universities for Research in Astronomy, Inc. (AURA), under contract AST–74–04129 with the National Science Foundation.

Appendix A

The electron impact correction to the wings of the hydrogen line profiles obtained from quasi-static ionic broadening is obtained by multiplying the wings of these profiles by a factor (Griem, 1974, p. 237) given in cgs units as

$$\Phi = \left(1 + \frac{5}{2}\pi \frac{C_{n'n}}{|\alpha|^{3/2}}\right)\left(\frac{4}{\pi}\right)^{3/2} Y_{n'n}^{1/2}\left(\frac{1}{2}\exp(-Y_{n'n}) + \right.$$
$$\left. + \frac{4}{3}\frac{kT}{E_H}\exp(-Y_{n'n})\right) . \qquad \text{(A.1)}$$

© Kluwer Academic Publishers • Provided by the NASA Astrophysics Data System

1983SoPh...83...83F

Here

$$C_{n'n} = 6.1 \times 10^{-7} \frac{n^3 n'^6}{\left[1 - \left(\frac{n'^2}{n^2}\right)\right]^{3/2}} \tag{A.2}$$

is an approximation to the quasi-static ion broadening profile. The function $Y_{n'n}$ is computed in cgs units from

$$Y_{n'n} = 10^8 \frac{(n^2 - n'^2)\pi\hbar c E_0 |\alpha|}{\lambda^2 kT}, \tag{A.3}$$

where all symbols have their usual meanings, and E_0 is the Holtsmark field described previously.

This asymptotic formula for the correction to the profile wings is valid (Griem, 1974, p. 239) at distances from the line center given by

$$\alpha \geq 7 \times 10^{-4} \frac{n^2 n'^4}{\left(1 - \frac{n'^2}{n^2}\right)}. \tag{A.4}$$

For the high Balmer lines of interest here, (A.4) implies that use of (A.1) is justified at values of $\alpha \gtrsim 3.5$, or $\Delta\lambda \gtrsim 0.3$ Å from the line core. Nevertheless, the contribution to the width of the total convolved profile $\Delta\lambda_{1/2}$ due to this correction, is found to be as large as 15%, and thus cannot be neglected.

We have found that additional multiplicative terms correcting for e.g. charge shielding and particle correlation effects, also given by Griem (1974) can be neglected in this analysis of coronal Balmer lines. Their effect on the halfwidths is below 5%, thus below the level of measurement errors on high-n lines in this study. Our results using these formulae agree closely (to within a factor 2 in density) with our reduction of the same data using the formula given by Kurochka (1969), and used by Rosenberg *et al.* (1977) in their analysis of Stark effect at the limb over quiet and active regions.

Appendix B

To derive a lower limit to the integral in Equation (4), for the case of a scattering electron located at a height h above the photosphere, we: (a) calculate the solid angle included by the photospheric horizon as viewed from the electron; (b) replace $I(\omega)$ by a lower limit based on the Eddington limb darkening approximation; and (c) replace the anisotropic dipole scattering term $(1 + \cos^2\gamma)$ by its lower limit of unity.

In the first step (a) we calculate the angle ϕ (Figure 5) at the electron, between the local vertical and the photospheric horizon. This is

$$\phi = \sin^{-1}[R/(R + h)] \tag{B.1}$$

© Kluwer Academic Publishers • Provided by the NASA Astrophysics Data System

1983SoPh...83...83F

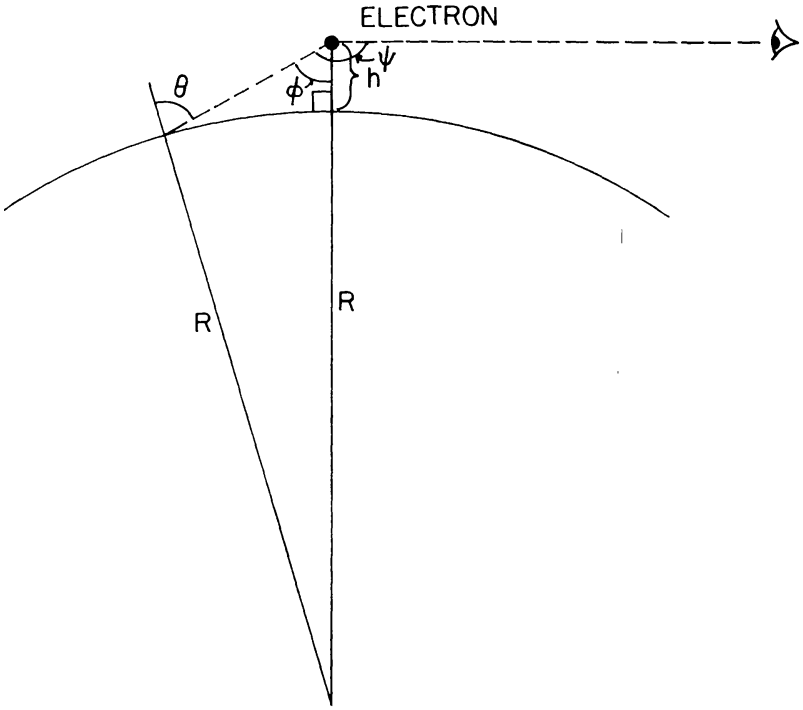

Fig. 5. Geometry used to derive the Thomson scattering intensity from an electron located at a height h above the photosphere.

in terms of h and the solar radius R. For a typical loop height $h = 5 \times 10^4$ km, we find $\phi = 69°$. The solid angle subtended by the photosphere is then

$$\omega = 2\pi \int_0^{69} \sin\phi \, \mathrm{d}\phi \simeq 4 \text{ sr} .$$

In step (b), we have from the Eddington approximation to limb darkening in terms of $\mu = \cos\theta$:

$$I(\mu)/I(1) = 3/5(\mu + \tfrac{2}{3}) . \tag{B.2}$$

It follows that at the horizon, for $\theta = \pi/2$, we have $I(0) = 0.4I(1)$. We take this value $0.4I(1)$ as a lower limit to $I(\omega)$ in Equation (4).

With these two approximations, and the lower limit $(1 + \cos^2\theta) > 1$, we can rewrite Equation (4) as

$$I_s \gtrsim 6.4 \times 10^{-27} (\bar{n}_e L) I(1) . \tag{B.3}$$

Finally, the intensity $I(1)$ seen at photospheric disc center from the electron can be related to the mean solar disc intensity, to which our calibrations refer, by simple integration of the Eddington limb-darkening approximation, yielding $\bar{I}_\odot = 0.8I(1)$. With this substitution, (B.3) can be written as the upper limit on $\bar{n}_e$ that we seek, namely:

$$\bar{n}_e \lesssim \frac{1.3 \times 10^{25}}{L} \frac{I_s}{I_\odot} . \tag{B.4}$$

© Kluwer Academic Publishers • Provided by the NASA Astrophysics Data System

1983SoPh...83...83F

References

Alfvén, H.: 1977, *Rev. Geophys. Space Phys.* **15**, 271.
Cheng, C.: 1980, *Astrophys. J.* **238**, 743.
Chevalier, R. and Lambert, D.: 1970, *Solar Phys.* **11**, 243.
Davis, W.: 1977, *Solar Phys.* **54**, 139.
Dere, K.: 1982, *Solar Phys.* **75**, 189.
Dunn, R., Evans, J., Jefferies, J., Orrall, F., White, O., and Zirker, J.: 1968, *Astrophys. J. Suppl.* **15**, 279.
Feldman, U. and Doschek, G.: 1977, *Astrophys. J.* **212**, 913.
Fisher, R.: 1974, *Solar Phys.* **35**, 401.
Foukal, P.: 1975, *Solar Phys.* **43**, 327.
Foukal, P.: 1976, *Astrophys. J.* **210**, 575.
Foukal, P.: 1978, *Astrophys. J.* **223**, 1046.
Griem, H.: 1960, *Astrophys. J.* **132**, 883.
Griem, H.: 1974, *Spectral Line Broadening by Plasmas*, Academic Press.
Hinata, S.: 1979, *Astrophys. J.* **232**, 915.
Hinata, S.: 1981, preprint.
Hirayama, T.: 1961, *Publ. Astron. Soc. Japan* **13**, 152.
Hirayama, T.: 1963, *Publ. Astron. Soc. Japan* **15**, 122.
Holtsmark, J.: 1919, *Ann. Phys.* **58**, 577.
Ivanov-Kholodnyi, G.: 1959, *Astron. Zh.* **36**, 589.
Jefferies, J. and Orrall, F.: 1958, *Astrophys. J.* **127**, 714.
Jefferies, J. and Orrall, F.: 1961, *Astrophys. J.* **133**, 946.
Jordan, C., Bartoe, J. D., and Brueckner, G.: 1980, *Astrophys. J.* **240**, 702.
Kopp, R. and Pneuman, G.: 1976, *Solar Phys.* **50**, 85.
Kurochka, L.: 1969, *Soviet Astron.* **13**, 64.
Levine, R. and Withbroe, G.: 1977, *Solar Phys.* **51**, 83.
Petrasso, R., Nolte, J., Gerassimenko, M., Krieger, A., Krogstad, R., Seguin, F., and Švestka, Z.: 1979, *Solar Phys.* **62**, 133.
Redman, R. and Suemoto, Z.: 1954, *Monthly Notices Roy. Astron. Soc.* **114**, 238.
Rosenberg, F., Feldman, U., and Doschek, G.: 1977, *Astrophys. J.* **212**, 905.
Stern, D.: 1977, *Rev. Geophys. Space Phys.* **15**, 156.
Švestka, Z. and Fritzová-Švestková, L.: 1967, *Solar Phys.* **2**, 75.
Underhill, A. and Waddell, J.: 1959, NBS Circ., No. 604.
Vernazza, J., Avrett, E., and Loeser, R.: 1981, *Astrophys J. Suppl.* **45**, 635.

© Kluwer Academic Publishers • Provided by the NASA Astrophysics Data System